LAWRENCE
LIVERMORE
NATIONAL
LABORATORY

LLNL-JRNL-635642

Contrasting Behavior of GaP(001) and InP(001) at the Interface with Water

B. C. Wood, E. Schwegler, W. I. Choi, T. Ogitsu

April 22, 2013

Journal of the American Chemical Society

Disclaimer

Contrasting behavior of GaP(001) and InP(001) at the interface with water

Brandon C. Wood,[1, a)] Eric Schwegler,[1] Woon Ih Choi,[1] and Tadashi Ogitsu[1]
Quantum Simulations Group, Lawrence Livermore National Laboratory, Livermore, CA 94550

We perform large-scale *ab initio* molecular dynamics simulations of the water/semiconductor interface for pristine, oxygen-rich, and hydroxyl-rich (001) surfaces of InP and GaP photoelectrodes. Our simulations show that even small concentrations of surface-adsorbed oxygen can promote self-sustaining, spontaneous dissociative adsorption of water, causing electrode surfaces to become densely covered with hydroxyls and other hydrogen-bonding species. A detailed analysis of the resulting network structure and composition reveals a richly dynamic chemistry, driven by solvent fluctuations and characterized by local proton transfer and rapid hydrogen-bond breaking. Despite their structural and electronic similarities, InP and GaP demonstrate qualitatively different interfacial dynamics. This can be traced to a more rigid hydrogen-bond network for GaP, which limits the explored topological phase space. As a consequence, local proton hopping can give rise to long-range surface proton transport on InP, whereas the process is kinetically limited on GaP. Possible implications for the kinetics of cathodic water splitting and photocorrosion on the two surfaces are evaluated in light of available experimental evidence.

I. INTRODUCTION

Photoelectrochemical cells promise sustainable production of hydrogen from water using solar energy[1]. In these devices, photogenerated carriers are responsible for driving the water redox reaction at the interface between the semiconductor electrode surface and an electrolyte solution[2–4]. Of the available semiconductor electrode materials, polar surfaces of Group-III phosphides currently show the highest reported hydrogen evolution activity; however, the durability of the electrode surfaces under operating conditions remains a significant impediment[5–11]. In order to improve photoelectrode stability and reactivity, as well as to optimize the alignment of the surface band edges, it is crucial to obtain a detailed understanding of the dynamical structure of the interface, the nature of the surface states, and how these states are modulated by the addition of the electrolyte solution[1,3].

Oxygen-derived adsorbates are known to be present on realistic III-V surfaces, even after surface cleaning[9,12–14]. These are thought to significantly modify the surface states that act as precursors to photoillumination[8,14–18]. The importance of considering these adsorbates in III-V surface models was borne out in our previous analysis of oxygen and hydroxyl adsorption on Ga/In-rich GaP(001) and InP(001) under vacuum conditions[19]. The (001) surface was chosen because it is preferentially exposed during epitaxial growth on existing (001)-oriented substrates[11]. It is also intrinsically polar, which enhances chemical interaction with the electrolyte. Our study found that surface binding of oxygen-derived adsorbates is thermodynamically favorable and can significantly modify the band edges, which has potential relevance for electrode stability. We also showed that despite the complex variety of morphologies reported in the literature, the fundamental electronic properties of the adsorbate-decorated surface correlate well to the local oxygen bond topology. As such, we concluded that the fundamental electronic and chemical properties of complex oxygen-containing GaP/InP(001) surfaces can be qualitatively reproduced by compositing local bond topologies. From a wide range of tested surface structures, we identified the two most prevalent and energetically favorable oxygen bond topologies (M–O–P and M–O–M, where M=[In,Ga]) and hydroxyl bond topologies (M–OH and M–[OH]–M)[19]. These were suggested as viable prototypes for further surface studies.

In this paper, we use the three surface bond topologies (M–O–M, M–OH, and M–[OH]–M) as representative models to explore the properties of oxygen- and hydroxyl-rich GaP/InP(001) surfaces in a more realistic simulation environment that explicitly includes the dynamics of the water interface. Results are compared to full interfacial dynamics of the pristine GaP/InP(001) surface to formulate a more complete picture. We have chosen not to address the M–O–P topology, which incorporates oxygen into the subsurface rather than the surface. This is because subsurface oxygen is unlikely to interact strongly with water, as we previously demonstrated.[20]

When compared with pristine GaP/InP(001), we show that oxygen and hydroxyl surface adsorbates significantly alter the chemistry of the interface, and that hydrogen bonding between the water and the semiconductor surface is especially important for describing the interfacial structure and dynamics. Moreover, we find that GaP and InP demonstrate qualitatively different hydrogen-bonding behavior, which manifests macroscopically and provides a possible interpretation of experimental results. Beyond the direct applications to photoelectrochemical hydrogen production, our results offer a fundamental study of a model polar surface in contact with water.

[a)] Electronic mail: brandonwood@llnl.gov

II. COMPUTATIONAL DETAILS

Car-Parrinello molecular dynamics simulations[21] were run within the canonical *NVT* ensemble using the Quantum-ESPRESSO code[22]. A fictitious electronic mass of 700 a.u. and a time step of 12 a.u. were used. Deuterium was substituted for hydrogen to permit the larger values. Accordingly, the term "hydrogen" should be assumed to refer to deuterium throughout the text. Temperatures were maintained using a chain of four Nosé-Hoover thermostats[23] with frequencies of 10, 20, 35, and 50 THz. Simulations were run at 400 K in order to properly reproduce the structural properties of liquid water.[24] Ultrasoft pseudopotentials[25] were used for all elements, and semi-core *d* states were included in the valence descriptions for indium and gallium. Cutoffs of 30 Ry and 300 Ry were used for the wave functions and charge density, respectively. The Perdew-Burke-Ernzerhof (PBE) exchange-correlation functional[26] was adopted for suitable description of the hydrogen bonds[27].

The semiconductor-water interface was generated using seven semiconductor layers oriented along (001), with periodic boundary conditions imposed. We used 16 semiconductor atoms per layer, in addition to any surface adsorbate atoms. Top and bottom layers were identically terminated to minimize spurious interactions between periodic images. Exposed surfaces were assumed to be In/Ga-rich, motivated by the preferential oxygenation of this surface over the P-rich surface[18]. Supercell axes were aligned along the [110], [$\bar{1}$10], and [001] directions. A total of 142 water molecules were inserted between periodic slab images, with the spacing adjusted to recover the experimental density of liquid water in the region center ($\sim$ 1.65 nm water thickness). Initial configurations were derived using classical TIP4P-generated bulk water[28], placed at the interface and equilibrated for 1 ps of *ab initio* dynamics with the surface degrees of freedom frozen. An additional 3 ps of equilibration was then performed with full degrees of freedom. Production runs were 20 ps. Statistics were averaged over the top and bottom surfaces of each semiconductor slab.

Three representative water/semiconductor interface simulations were run for each of the semiconductor materials InP and GaP. The first was a pristine (001) surface exhibiting the mixed-dimer $\delta(2\times4)$ reconstruction commonly observed for the In/Ga-rich (001) surface under ultra-high vacuum.[29] The second surface was constructed with surface *M*–O–*M* bridges, with oxygens occupying every other bridge site along [$\bar{1}$10] (0.5 ML coverage). The third was constructed by combining surface *M*–[OH]–*M* bridges with *M*–OH dangling-bond atop structures, with hydroxyl occupying every other bridge site along [$\bar{1}$10] and every atop site (1.5 ML coverage). The latter two configurations and accompanying coverages were derived from our earlier stability analysis.[19]

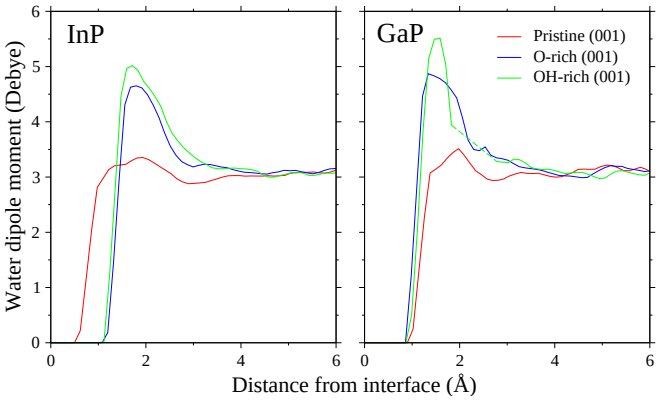

FIG. 1. Wannier function-derived water dipole moments as a function of distance from the water oxygen to the first full In/Ga-rich layer. Data is taken from the dynamics simulations of pristine mixed-dimer $\delta(2\times4)$, O-rich, and OH-rich InP(001) (left) and GaP(001) (right). For OH-rich GaP(001), the dashed line represents a linearly interpolated estimate in a region with zero water density.

III. RESULTS AND DISCUSSION

A. Molecular structure of interfacial water

We begin with a discussion of some underlying impacts of surface oxygen and hydroxyl on the molecular and electronic structure of water. One such impact is a significant enhancement of the average dipole moment of a water molecule as it approaches an InP/GaP(001) surface decorated with oxygen or hydroxyl. This can be seen in Fig. 1, which plots the dipole moment as a function of perpendicular distance from the surface. To calculate the dipole moments, we used maximally localized Wannier functions (MLWFs)[30,31] extracted from 15 uncorrelated simulation frames. The moments were calculated as the vector sum of the nuclear coordinates and the Wannier function centers (WFCs), with only intact water molecules included in the analysis. From Fig. 1, it is evident that surface oxygen or hydroxyl can dramatically enhance the average water dipole in the first 2 Å of water by more than 60%, signaling a fundamental shift in the water electronic structure in this region. By comparison, the dipole response of the pristine surface mixed-dimer $\delta(2\times4)$ surface is minor.

Accompanying the dipole enhancement is a reorganization of the charge density of water molecules at the interface. This can be seen upon examination of the distributions of WFCs and spreads for water oxygens, shown in Fig. 2. For reference, distributions for bulk water feature two peaks: shorter spreads and longer distances between nuclei and Wannier functions are associated with O–H chemical bonds, and vice versa for non-bonded/hydrogen bond-acceptor oxygen electron pairs. The pristine mixed-dimer $\delta(2\times4)$ surface largely retains these bimodal distributions. However, Fig. 2 shows that

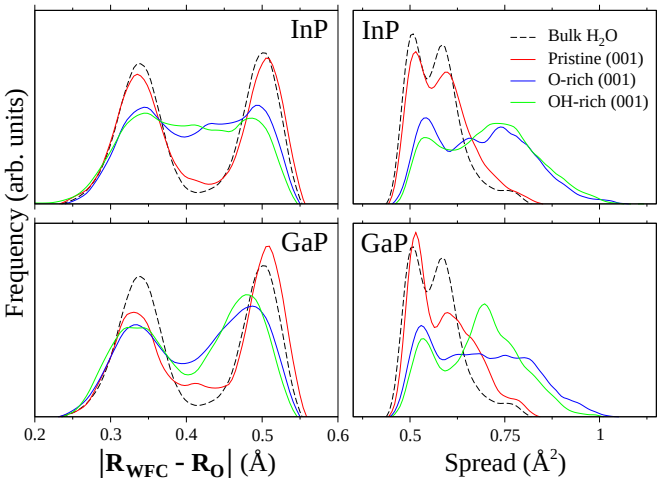

FIG. 2. Distribution of the centers (left) and spreads (right) of the maximally localized Wannier functions associated with oxygens of molecular water adsorbed on the surface during the course of the interface dynamics. Separate distributions are shown for pristine mixed-dimer $\delta(2\times4)$, O-rich, and OH-rich InP(001) (top) and GaP(001) (bottom). The dashed line is the value for the bulk-like water region midway between periodic surface images.

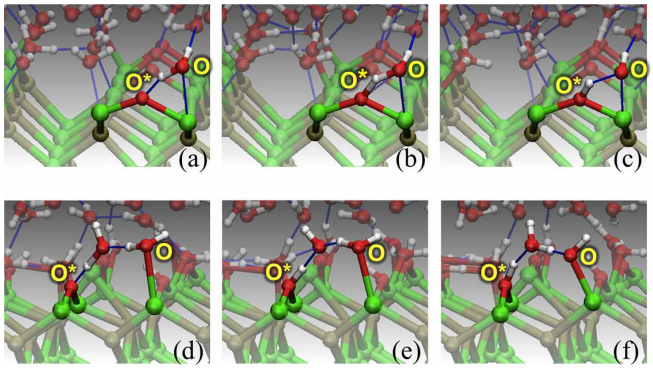

FIG. 3. Two alternative mechanisms for water dissociation at surface oxygen bridges on InP(001). O and O* refer to proton donor and acceptor oxygens, respectively. (a–c) The first scenario features a donor water molecule bound to one of the edge In atoms adjacent to O*, and transferring a proton across the O–H···O* complex. (d–f) The second scenario has the donor water molecule bound to an In atom that is not part of the In–O*–In bridge. In this instance, water molecules in solution act as intermediaries in a Grotthuss chain for site-to-site proton transfer. Color scheme: O=red, H=white, In=green, P=gray.

addition of surface O or OH tends to break down the bimodality, blurring the electronic distinction between O–H chemical and O···H hydrogen bonds. The distribution of spreads also broadens significantly, indicating increased delocalization of electrons across chemical and hydrogen bonds. Taken together, these effects point to decreased covalency in the O–H chemical bonds, accompanied by increased hydrogen-bond strength.

Note that the dipole enhancement (Fig. 1) and blurring of the distinction between hydrogen and chemical bonds (Fig. 2) do not manifest appreciably in the pristine surface, despite the fact that the pristine surface also carries a significant surface dipole. This means that in all likelihood, the changes in the molecular and electronic structure of water are not surface dipole induced. Rather, they are a direct consequence of unusually strong surface hydrogen bonding with adsorbates and with neighboring water molecules, which is largely absent for the pristine surface. This manifests as dramatically increased hydrophilic character, and turns out to have profound implications for the structure and chemistry of the interface.

B. Surface chemistry

Water adsorption in the presence of surface oxygen or hydroxyl leads to the formation of interfacial hydrogen bonds. Within the resulting surface O–H···O complexes, the weakening of the O–H chemical bond and strengthening of the O···H hydrogen bond results in low barrier for Grotthuss-type exchange of chemical and hydrogen bonds.[32] This manifests in the simulations as frequent local proton transfer at the interface with O- or OH-rich InP/GaP(001), limited to the region within 4 Å of the surface. Similar local proton-hopping behavior has been mentioned in the context of several other interfacial systems.[33–41]

In the presence of surface oxygen on InP(001) or GaP(001), we find that local proton transfer can lead to rapid, spontaneous dissociative adsorption of water molecules. The reactivity of surface oxygen towards water dissociation is a reflection of its electronic structure, which differs significantly from inert subsurface oxygen.[20] In the dynamics, an M–O–M bridge oxygen acts as the proton acceptor, and dissociation proceeds via one of two classes of competing mechanisms. These are shown schematically in Fig. 3. The first mechanism (Fig. 3a–c) is a local event in which both the proton donor and acceptor are anchored to the same In/Ga atom. The oxygen of the water molecule binds to the edge of the M–O–M bridge, with one O–H forming a hydrogen bond with the bridge oxygen. The hydrogen bond rotates the water dipole away from the surface normal direction, aligning the O–H···O complex and shortening the proton-transfer path.

The second mechanism for dissociative adsorption of water on M–O–M bridges is shown in Fig. 3d–f. In this case, proton donor and acceptor oxygens are bound to different In/Ga atoms. These are often connected by a Grotthuss chain[32] involving one or more water molecules in solution. The chain has a low barrier for proton diffusion, which proceeds via the Grotthuss mechanism as coordinated jumps across successive O–H···O complexes.

Interestingly, water dissociation via the second mechanism in Fig. 3d–f appears to be reversible. Although much rarer than the forward reaction, we nevertheless directly observe deprotonation of surface M–[OH]–M bridges to reform M–O–M. This means that both the protonation and deprotonation reactions are kinetically and thermodynamically accessible in the simulations.

Overall, the first mechanism is more common on InP(001) than on GaP(001), whereas the second mechanism is more common on GaP(001) than on InP(001). Nevertheless, the result of both water dissociation mechanisms is local hydroxylation of the surface, with the original water site now carrying an dangling-bond atop hydroxyl (M–OH), and the target site carrying a bridge hydroxyl (M–[OH]–M). Accordingly, in the absence of competing pathways, the initial presence of oxygen bridge topologies should lead to preferential surface hydroxylation in water. This is similar to the common behavior of oxide surfaces.

The fact that we do not observe dissociative adsorption of water on the pristine surface suggests that a surface adsorbate is necessary for favorable dissociation kinetics on InP/GaP(001) at zero bias. In this respect, our surface oxygen results are consistent with simulations of water dissociation on InP(100) in the presence of surface hydrogen.[42] However, this differs from the (110) surface of GaP/InP, where water dissociation reportedly proceeds unaided.[41,43].

For additional insight into the thermodynamics and kinetics of the dissociative water adsorption, we performed total-energy and nudged elastic band (NEB)[44] calculations of gas-phase water binding and dissociation on pristine and oxygen-decorated mixed-dimer $\delta(2 \times 4)$ surfaces.[45] The results are listed in Table I. For these estimates, only the first mechanism in Fig. 3a–c is considered, since results are more likely to be transferrable from the gas phase. The pristine surface shows a high kinetic barrier for dissociation of an adsorbed water molecule (0.71–0.82 eV). This is substantially lowered (0.04–0.16 eV) upon adsorption of surface oxygen. Moreover, the surface binding energy of an undissociated water molecule on the pristine surface is significantly weaker, and is probably in close competition with the water solvation energy. Also, dissociation of an adsorbed water molecule on the pristine surface is actually endothermic on InP (+0.14 eV) and only weakly exothermic (−0.16 eV) on GaP, whereas the thermodynamic driving force for dissociation is strong if oxygen is present. Our calculated dissociation energy is somewhat smaller in magnitude than the value reported by Jeon *et al.*[46]; nevertheless, molecular binding energies are in good agreement, and we are able to provide additional data on the kinetic barriers.

The mechanisms shown in Fig. 3 assume the proton acceptor is a bridge oxygen (M–O–M). However, we also observe analogous water dissociation reactions in which an atop hydroxyl group (M–OH) acts as the proton acceptor. These are also reversible, permitting both protonation and deprotonation. The net result in this case is the formation of a new water molecule at a different surface site, which conserves the total number of water molecules. Schematically, the bridge oxygen and atop hydroxyl proton-acceptor reactions can be expressed as follows:

$$M\text{–OH}_2 + M\text{–O–}M \longleftrightarrow M\text{–OH} + M\text{–[OH]–}M, \quad (1)$$

$$M\text{–OH}_2 + M\text{–OH} \longleftrightarrow M\text{–OH} + M\text{–OH}_2. \quad (2)$$

Note that an atop M–OH complex is both a product of the forward reaction of Equation 1 and a reactant in the forward reaction of Equation 2. In this way, dissociation products will promote further dissociation.

Because dissociative water adsorption preferentially converts surface oxygen to surface hydroxyl, we can restrict our further analysis to the initially hydroxylated surface without loss of generality. Results for the initially oxygen-rich surface are expected to be very similar once the interface has fully equilibrated.

There is a subtle but important distinction between local site-to-site proton transfer of the sort shown in Fig. 3 and actual long-range hydrogen transport. Specifically, local transfer will translate into long-range transport only if the involved hydrogen-bonded complexes can reorganize themselves dynamically between proton-transfer events. The variation in the donor-acceptor combinations guarantees topological diversity, ensuring that the proton does not simply hop back and forth between a small number of configurations. This highlights the importance of the structure and dynamics of the hydrogen-bond network, which are explored in detail below.

TABLE I. Energetics of initial surface binding (E_b) and subsequent dissociative adsorption ($E_\mathrm{diss} = E - E_\mathrm{b}$) of a single gas-phase water molecule on pristine mixed-dimer $\delta(2\times4)$ and oxygen-adsorbed GaP/InP(001). NEB-derived kinetic barriers for dissociation (ΔE_a) are also given. For the mixed-dimer $\delta(2\times4)$ surface, dissociation is assumed to occur on the M–P surface dimer, with OH binding to the M site, and H to the P site. For the O-rich surfaces, the mechanism of Fig. 3a–c is assumed. For E_diss and E_b, negative energies imply exothermic reactions.

Surface	E_b (eV)	E_diss (eV)	ΔE_a (eV)
InP $\delta(2\times4)$	−0.32	+0.14	0.82
GaP $\delta(2\times4)$	−0.37	−0.16	0.71
InP (O-rich)	−0.65	−0.61	0.04
GaP (O-rich)	−0.71	−0.54	0.16

C. Network structure and composition

Under sufficiently dense adsorbate coverage, the surface nucleates the formation of a well-defined interfacial

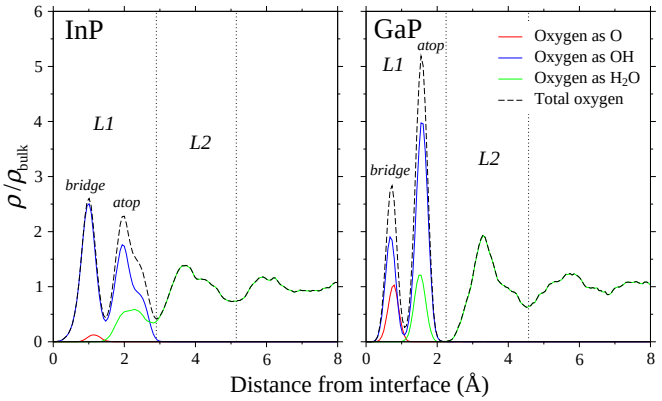

FIG. 4. Density of O, OH, and HOH moieties as a function of distance from the first full In/Ga-rich layer. Data is taken from the dynamics of the OH-rich surfaces. The total density of oxygen is shown as a dashed line. Boundaries for the $L1$ and $L2$ regions are delineated by dotted lines.

hydrogen-bond network. In practice, thermal motion and reversible local proton transfer create a dynamic equilibrium with the solvent environment. Accordingly, component surface structures may include bridge oxygens and molecular water, in addition to hydroxyl groups. The average surface concentrations of each which will be dictated by the equilibrium interfacial properties.

In order to identify and map the component structures involved in hydrogen bonding, we examine the individual spatial densities of oxygens with different numbers of attached protons in Fig. 4.[47] In this way, we can distinguish between O, OH, and H_2O at the interface. Looking first at the overall density of oxygen as a function of distance from the interface, we isolate two regions of particular interest for further analysis. The first region ($L1$) represents the surface adsorbate layer, which can be further decomposed into bridge and atop configurations by noting their direct correspondence with the first two sets of oxygen-derived peaks in Fig. 4. Categorizing atop and bridge bonds separately enables us to confirm that a lone surface oxygen occurs uniquely as a bridge bond (M–O–M), water as an atop bond (M–OH_2), and hydroxyl as either configuration (M–[OH]–M, M–OH). The second region ($L2$) is the first interfacial solvent layer, in which nearly all oxygens exist as water molecules. Although we focus our analysis on the $L1/L2$ region, we point out that clear fluctuations in the oxygen density are observable beyond the $L2$ boundary. This underscores the value of accounting for the full solvation environment in lieu of a simpler model based only on a $L1$–$L2$ water bilayer.

A well-defined boundary exists between $L1$ and $L2$ in Fig. 4. This is similar to the behavior reported for other hydrophilic systems, including SiC(001)[48] and TiO_2.[49] However, the boundary is noticeably more pronounced for GaP than for InP. In fact, there is zero oxygen density in the $L1/L2$ boundary region of GaP, meaning water molecules are *never* exchanged between the surface adsorbate layer and the solvent once the interface has equilibrated. In contrast, the $L1/L2$ interface for InP appears to be much more fluid.

Similarly, the gap between the atop and bridge hydroxyl peaks of $L1$ in Fig. 4 is much deeper for GaP than for InP. The region between the peaks is traversed upon transition between the atop and bridge bond types, which occurs by breaking or forming one of the M–OH bonds in the bridge. Accordingly, we infer that topological interchange of atop and bridge hydroxyls is much less frequent for GaP. The $L1$ and $L2$ layers are also much narrower for GaP than for InP, as are the distributions of oxygen density within each layer. Together, these features support the interpretation of a more rigid, well-defined network structure at the interface with GaP.

Within $L1$, where the identity of the surface species varies, we can integrate over the peaks in Fig. 4 to obtain the relative likelihood of the bridge oxygen (M–O–M), atop hydroxyl (M–OH), bridge hydroxyl (M–[OH]–M), and atop water (M–OH_2) bond types. The normalized fractions of each type are shown in Table II. We have also translated these values into estimated differences in free energy at the given simulation temperature.

Based on the $L1$ concentrations in Table II, it is immediately evident that the M–[OH]–M bridge and the atop M–OH comprise the primary building blocks of the hydrogen-bond network at the surface. However, bridge oxygens and atop water molecules also appear in non-negligible concentrations. The importance of the solvent is implicit in the results: the computed free energy differences of the bond topologies in Table II have a spread that is much smaller than the reported spread of zero-temperature energies in the absence of liquid water[19] (tens of meV, rather than hundreds of meV). For example, consider that the zero-temperature formation energy of a M–[OH]–M bridge at the vacuum interface is lower than that of an atop M–OH by 510 meV (300 meV) for InP (GaP) when averaged over unique surface configurations in Ref.[19]. Nevertheless, when the finite-temperature solvent is included, the atop M–OH features prominently, and the free-energy difference becomes very small. This means that the degree of solvent-driven stabilization depends on the bond type. In the case of atop hydroxyl, preferential stabilization is likely traceable to increased favorability for hydrogen bonding. This is a consequence of the atop hydroxyl being able to accept an additional hydrogen bond, as well as its having less steric hindrance.

Interestingly, significant differences are seen when comparing GaP and InP in Table II, which are signatures of fundamentally different network compositions. For instance, in the case of InP, the bridge and atop topologies appear with near-equal likelihood, whereas for GaP, there is more than a two-to-one preference for atop M–OH. This may be a factor in the more rigid network for GaP in the $L1$ region, since atop hydroxyls can also accept hydrogen bonds and generally interact more strongly with the $L2$ solvent layer due to proximity. Another difference is that the relative likelihood of finding lone surface

TABLE II. Relative percent of oxygens in the $L1$ region of OH-decorated InP/GaP(001) that correspond to each of the four dominant surface oxygen-containing bond types. Also listed are the corresponding estimated free energy differences ΔF with respect to the highest-concentration bond topology, assuming the system is in equilibrium.

Bond Type	InP (%)	ΔF (meV)	GaP (%)	ΔF (meV)
M–O–M	1.7	+109	11.8	+51
M–[OH]–M	40.5	+0	21.8	+30
M–OH	39.5	+1	51.4	+0
M–OH_2	18.2	+28	15.1	+42

bridge oxygens not bonded to protons is nearly six times greater for GaP than for InP. This has possible implications for corrosion mitigation if these bridges contribute to photocorrosion via hole trapping, as we have previously postulated.[19]

D. Network connectivity and topology

Although Fig. 4 illustrates which oxygen-derived surface and interface components comprise the hydrogen-bond network, it does not illustrate the connectivity of that network. It also does not distinguish between hydrogen bonds formed within a layer, bonds formed to the next outer layer, and bonds formed to the next inner layer. For this, we need a full spatial density of map of hydrogen bonds, resolved by location of both donor and acceptor oxygens. This is shown in the planar-averaged density contours of Fig. 5a–b. We have also performed a similar analysis for the density of hydrogen-bond breaking (Fig. 5c–d), which gives a measure of which hydrogen bonds are likely to break or remain intact.

The local maxima in Fig. 5a–b represent the most frequent donor-acceptor combinations for InP and GaP. As expected, hydrogen bonds between $L1$ (bridge and atop) and $L2$ are common, as are bonds between two $L1a$ (atop) oxygens (particularly for GaP). Overall, however, InP demonstrates far greater topological variety. For instance, InP also shows hydrogen bonding between $L1b$ (bridge) and $L1a$ (atop), and even directly between two $L1b$ bridges.

Comparing the overall hydrogen-bond density contours (Fig. 5a–b) with the density contours of hydrogen-bond breaking (Fig. 5c–d) reveals some additional surprises. For instance, hydrogen bonds from $L1b$ (bridge) to $L1a$ (atop) break most commonly for InP, despite the fact that the $L1b \rightarrow L1a$ bond is not a particularly prevalent bond type. For GaP, $L1a$–$L1a$ bond breaking entirely dominates, but to an even greater degree than one might expect from an examination of the overall density contours. This likely relates to the especially high rate

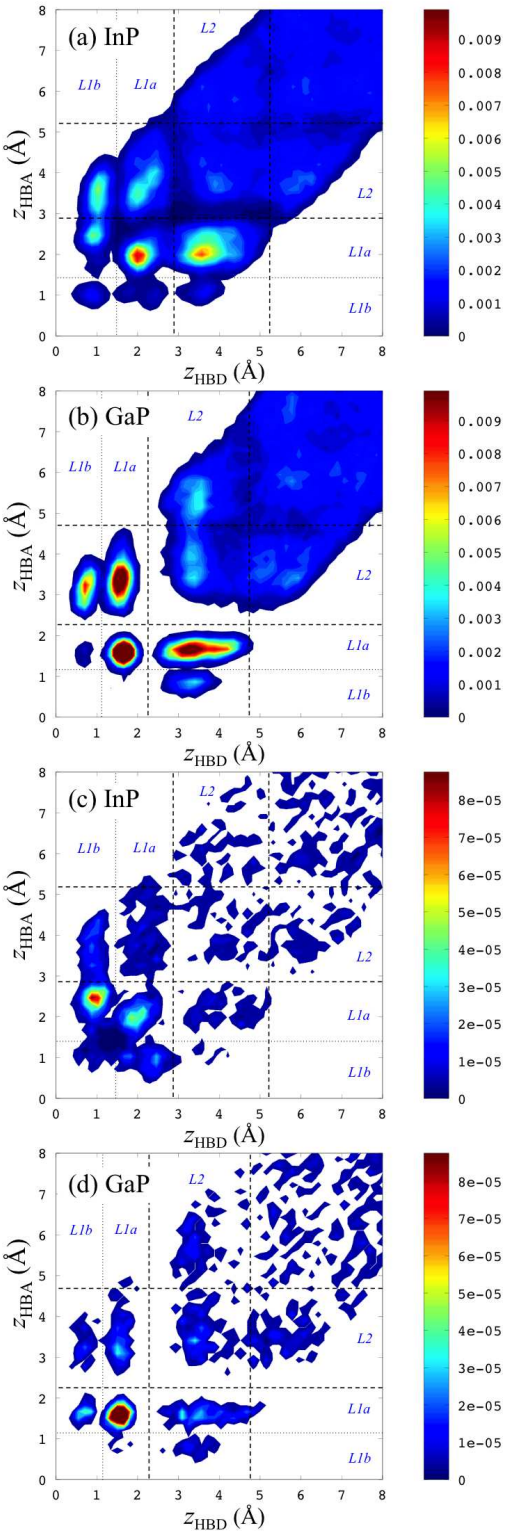

FIG. 5. Planar-averaged density contours ($Å^{-3}$) of hydrogen bonds in the hydroxylated surface simulations, indexed by the position z of the hydrogen-bond donor (HBD) and acceptor (HBA) oxygens, measured perpendicular to the interface. Panels (a) and (b) show the overall hydrogen-bond density for InP and GaP, respectively; (c) and (d) show the density of broken hydrogen bonds. Whitespace means zero density. $L1b$ and $L1a$ refer to the bridge and atop peaks in Fig. 4.

of proton exchange between neighboring $L1$ atop groups that we observe for GaP, which simultaneously breaks hydrogen bonds. We also observe significantly enhanced hydrogen bond density for GaP between two $L2$ oxygens, as well as from $L2$ oxygens to oxygens farther from the interface. This may be a consequence of the gap in oxygen density between $L1$ and $L2$ for GaP.

The area of phase space that is spanned by each of the local wells in Fig. 5 is physically related to the rigidity or fluidity of the corresponding hydrogen-bond network component. Comparing the contour maps for InP (Fig. 5a) and GaP (Fig. 5b), it is immediately evident that the configurational free-energy surface for hydrogen bonds, as parametrized by donor and acceptor position, is substantially flatter for InP than for GaP. This is clear from the sharpness of the peaks in the density profile of GaP, as well as the generally smaller area of phase space that is associated with each. This implies that the hydrogen-bond network in the interfacial region is significantly more structured and rigid for GaP, similar to what we concluded based on Fig. 4. Some structure is even observable in the density of GaP $L2$ oxygens donating hydrogen bonds to layers farther from the interface.

The frequented regions of phase space in the interfacial region (bonds involving only $L1$ and $L2$ donors and acceptors) in Fig. 5 are largely disconnected in the case of GaP but are continuous for InP. Connectedness is related to the capability of the hydrogen-bond network to interchange between topologies. This can happen in one of two ways: either the oxygen donor/acceptor migrates between layers (keeping the network otherwise intact), or else a hydrogen bond of one topology is broken and then reformed to an oxygen with a different topology. Within the interfacial region, there is some minor continuity between regions corresponding to $L1$ bridge and $L1$ atop donors/acceptors for GaP. This is an artifact of the interchange between bridge and atop hydroxyls described earlier in the context of Fig. 4, and shows up less prominently than for InP. Otherwise, any hydrogen-bond breaking and adsorbate reorganization events in the interfacial region of GaP occur only within their originally defined interfacial layer. This behavior is in sharp contrast to InP, which demonstrates continuity between nearly all regions of the interfacial hydrogen-bond configurational phase space. This means hydrogen bonds at the InP/water interface, in addition to their host oxygens, are being continually and fluidly exchanged between layers. The topological fluidity of InP over GaP is also clear in the hydrogen-bond breaking contour map (Fig. 5c–d).

The surface dynamics of GaP and InP offer insight into the underlying motivations behind the different fluidities of the interfacial hydrogen-bond networks. Two contributing factors are illustrated in Fig. 6. The first relates to the enhancement of the hydrogen-bond strength of $L1$ donors, which turns out to be larger for GaP than for InP. We can see this in Fig. 6a, which plots the vibrational density of states (VDOS) of hydrogens in $L1$, as calculated by taking the Fourier transform of the velocity

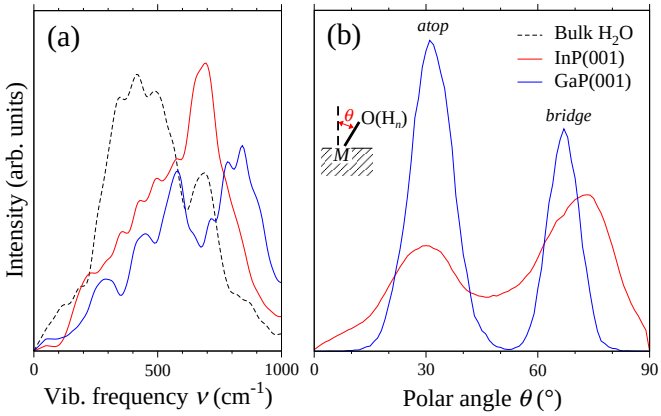

FIG. 6. (a) Vibrational density of states (VDOS) for hydrogen atoms in the $L1$ interfacial region of OH-adsorbed InP(001) and GaP(001), compared with atoms in the bulk-like water region midway between periodic surface images. (b) Distribution of the orientation of M–O bonds on OH-adsorbed InP(001) and GaP(001), measured as the polar angle with respect to the surface normal direction.

autocorrelation function. Here we have focused on the librational modes about hydrogen bonds, which dominate the spectrum below 1000 cm^{-1} and are a good indicator of hydrogen-bond strength and rigidity. The spectrum shifts towards higher frequencies when compared with the bulk-like water region, indicating stronger hydrogen bonds for both surfaces. However, the shift is noticeably larger in the case of GaP, in agreement with its observed rigidity.

The second factor relates to the softness of the In-derived surface modes, and to the corresponding strength and covalency of the Ga–O bond with respect to the In–O bond.[19] This is illustrated in Fig. 6b, which shows the orientations of M–O bonds at the surface, measured with respect to the surface normal. The distribution is bimodal, with low- and high-angle peaks corresponding to component atop (M–OH) and bridge (M–[OH]–M, M–O–M) structures, respectively. The distribution for InP is much broader than for GaP, indicating a softer and more fluid surface. Note that the low likelihood of intermediate angles for GaP translates to fewer interchanges between atop and bridge structures, consistent with our analysis of Figs. 4 and 5.

We can quantify the range of topological phase space spanned by the hydrogen-bond network dynamics by introducing an index that measures the diversity of hydrogen bonding configurations across simulation frames. To do so, we first introduce the adjacency matrix $\mathbf{A}$ to map the topology of the hydrogen-bond network within a directed graph-theoretic formalism.[50] Oxygens in the system are indexed $\{1, \ldots, N\}$, and the element $\mathbf{A_{ij}}$ of the $N \times N$ adjacency matrix is defined as one if oxygen i donates a hydrogen bond to oxygen j, and zero otherwise. Within this scheme, we can define a configurational entropy S of the explored phase space that is analogous

TABLE III. Calculated values of S for oxygen donor/acceptor combinations in the $L1$ and $L2$ interfacial regions of hydroxylated GaP(001) and InP(001). For reference, the computed value of S in the bulk-like water region is 5.78.

Bond type	InP(001)	GaP(001)
$L1 \rightarrow L1$	4.22	2.69
$L1 \rightarrow L2$	4.20	3.44
$L2 \rightarrow L1$	3.82	3.45
$L2 \rightarrow L2$	4.64	3.88

to the Shannon entropy in information theory:

$$S = -\sum_{ij}^{N} \langle \mathbf{P_{ij}} \rangle \ln \langle \mathbf{P_{ij}} \rangle \,, \text{ where } \langle \mathbf{P_{ij}} \rangle = \frac{\langle \mathbf{A_{ij}} \rangle}{\sum_{ij}^{N} \langle \mathbf{A_{ij}} \rangle}. \quad (3)$$

Here we have used angle brackets to denote averages over equilibrated simulation frames. The definition in Equation 3 can be easily restricted to donors and acceptors located within a user-definable region of space by including only those pairs in the calculation of $\langle \mathbf{A_{ij}} \rangle$. Physically, S relates both to the size of the topological phase space explored during the simulation, and to the uniformity of that phase space exploration. It will trend to larger values for networks of low topological diversity (sparse and nonuniform $\mathbf{A}$) and smaller values for networks of high topological diversity (dense and uniform $\mathbf{A}$). S is advantageous in that it maps the efficiency of phase space exploration not only between successive interfacial layers, but also *within* each layer.

Table III shows the computed values of S for all combinations of hydrogen bonds donated and accepted by the $L1$ or $L2$ regions. As expected, InP shows significantly higher topological diversity. This confirms that the topological phase space explored by the interfacial hydrogen-bond network of InP is much broader than for GaP, and that the exploration is relatively efficient and uniform across topological configurations.

According to Table III, the largest average difference between GaP and InP is seen for bonds wholly within $L1$. In this case, the value of S for GaP is particularly low, implying that the system shows very little topological variability. This is likely an artifact of the rigid atop-atop bonds for GaP, where repeated proton transfer induces hydrogen-bond breaking with very limited exploration of the phase space (see Fig. 5d). Significant differences between GaP and InP are also seen for $L1 \rightarrow L2$ and $L2 \rightarrow L2$ bonds. This means that GaP is poor at exchanging hydrogen bonds and water molecules between the surface network structure and the solvent, whereas InP does so with much greater ease.

E. Network dynamics and the role of the solvent

The previous sections have focused largely on characterizing the time-averaged properties of the hydrogen-bond network. We turn now to an analysis of specific reaction mechanisms for hydrogen-bond breaking. Within the $L1$ surface layer, such reactions are often connected to changes in hydrogen-bond composite structures that topologically bridge successive In/Ga surface atoms. Understanding the evolution of these composite bridging structures is especially important, since they comprise the key building blocks for the continuous, quasi-2D network that exists at the interface. They also form the basis for local proton-transfer reactions of the type shown in Fig. 3.

We begin by considering only those composite structures derived from surface hydroxyl groups, since these occur with the highest frequency and show the most topological diversity in possessing both bridge and atop surface configurations. A detailed analysis of the peaks in the contours of Fig. 5, combined with direct inspection of the network dynamics, allows us to identify four unique classes of hydroxyl-based component superstructures that topologically bridge neighboring In/Ga atoms in $L1$. Examples representing each class are shown in the lettered diagrams of Fig. 7. The four classes include: hydrogen bonding between adsorbates (complex a), shared hydrogens in a Zundel-like structure (complex b), bridging via solution molecules in Grotthuss chains (complex c), and direct bridging with a single adsorbate (complex d). For complexes a and c, either (or both) of the atop hydroxyls may be replaced by bridge hydroxyls oriented into the plane of the paper. Complexes a and b appear in our simulations along both the [110] and [$\bar{1}$10] crystallographic directions, whereas c aligns preferentially along the [110] direction, and d along the [$\bar{1}$10] direction. Note that structures analogous to those in Fig. 7 have been reported on other hydrophilic surfaces following water dissociation, including oxides,[38,51] metals,[40] and III-V semiconductors.[41,52]

It is in the dynamics of the composite bridging complexes of the types shown in Fig. 7 that the difference in fluidity of the GaP and InP hydrogen-bond networks becomes extremely relevant. This is because the interconversion between the hydroxyl-derived complexes is generally activated by dynamic exchange of H, OH, or H_2O elements between the surface ($L1$) and the solvent ($L2$) environments. Because $L1 \leftrightarrow L2$ interlayer solvent exchange is rare (or forbidden) at the structurally rigid GaP-water interface, these interconversion reactions are observed only in simulations of the more fluid InP network. As an illustration, some of the observed reaction pathways by which interconversion takes place on InP(001) are shown alongside the arrows in Fig. 7, with the relevant solvent exchange species highlighted in red.

As already discussed, the hydroxyl elements in Fig. 7 may also be dynamically converted into surface oxygen or water via local proton transfer across the bridg-

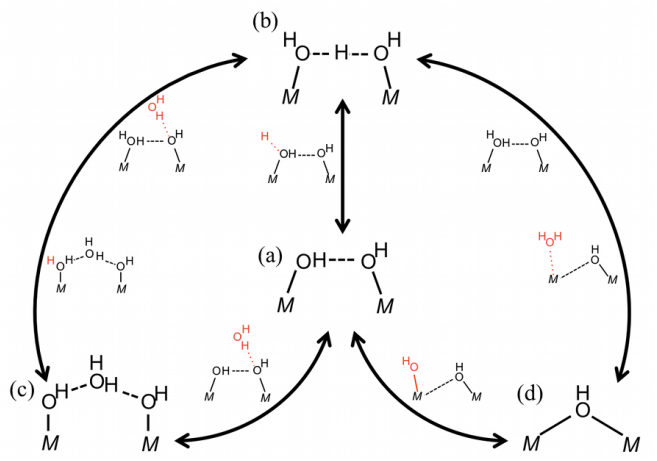

FIG. 7. Schematic illustrations of four OH-involving surface configurations that bridge neighboring M sites in the course of the dynamics simulations of OH-rich InP/GaP(001). Mechanisms by which the InP(001) surface interchanges these configurations are shown, with the solvent environment assumed to provide the atoms in red.

ing structures. In this case, atop hydroxyls (M–OH) act as Brønsted-Lowry bases to become surface-adsorbed molecular water (M–OH_2), and bridge hydroxyls (M–[OH]–M) act as Brønsted-Lowry acids to become bridge oxygens (M–O–M). Because local proton transfer need not involve solvent exchange, it is not forbidden by the comparatively rigid structure of the GaP-water interface. In fact, the rigidity of the GaP network statistically enhances local proton transfer, with local O–H bond breaking events occurring roughly twice as frequently for GaP as for InP. The disparity is likely due to a combination of longer average lifetime of highly aligned Grotthuss chains (Fig. 7c), as well as decreased exchange barrier due to stronger average hydrogen bonding.

The kinetics of hydrogen-bond network reorganization and local proton transfer appear to be in competition: the fluid network of InP favors the former, while the rigid network of GaP favors the latter. Nevertheless, InP still exhibits relatively facile site-to-site hydrogen transfer events (much faster than liquid water, for instance), whereas GaP shows extraordinarily limited network reorganization capability and kinetics, especially within $L1$. In this regard, InP achieves a superior balance between the two factors. Accordingly, one should expect that local proton hopping should translate to rapid, long-range surface hydrogen transport on InP(001), provided adsorbate concentration becomes high enough to topologically connect the surface hydrogen-bond network. Because all observed proton hopping events are confined to the interface, such long-range transport will be two dimensional. In contrast, local proton hops on GaP will be confined to a small region of phase space, preventing facile long-range transport. This is an instance in which minor differences in surface electronic structure generate qualitatively different macroscopic behavior.

We emphasize that solvent fluctuations are crucial for driving long-range interfacial hydrogen transport. These fluctuations are responsible both for the reorganization of the hydrogen-bond network and for inducing local proton hopping. This capability depends on the existence of a relatively flat free energy landscape, in which fluctuations in the instantaneous solvation energy are of the order of the energetic differences. For GaP/InP(001), the flatness of the landscape is aided by opposite heuristic trends in the solvation and formation energies. Relying on the formation energies calculated in Ref.[19] and ignoring direct adsorbate-adsorbate interactions, the general order of surface adsorbate stability is –[OH]– > –OH ⩾ –O– > $–OH_2$. On the other hand, if we use the number of possible hydrogen bonds with the solvent as an indicator of the solvation energy, this order is essentially reversed: $–OH_2$ (2 donors, 1 acceptor) > –O– (0 donors, 2 acceptors) = –OH (1 donor, 1 acceptor) > –[OH]– (1 donor, 0 acceptors). The competition between formation and solvation energies makes all four topologies realizable in the simulations, and local solvation fluctuations are large enough by comparison to generate temporary gradients for interchange. Note also that changes in pH and availability of solvent species are likely to shift reaction equilibria to favor formation of certain complexes over others.

The significance of the solvent in driving surface reactivity and hydrogen transport is addressed directly in Fig. 8. In it, we show the distributions of indium and water neighbor distances from a water molecule in the $L1$ region of the hydroxyl-adsorbed InP(001) interface. Two separate sets of distributions are shown: one for water molecules that are actively breaking or forming O–H bonds (sampled at $\Delta t = 10$ fs prior to the event itself), and another averaged over all remaining frames. When O–H bond breaking or forming is imminent, the mean nearest-neighbor distance to nearby waters is shortened by 0.25 Å, and the corresponding peak becomes much better defined. This means instantaneous solvent environments featuring unusually close intermolecular water distances are significantly more likely to induce hydrogen transport. In contrast, the distance to the nearest surface metal ion is similar whether or not an O–H bond breaking/forming event takes place. This confirms that the solvent environment is the most important determiner of the local chemical gradient that drives hydrogen transport. We should note that although the results of Fig. 8 are for $\Delta t = 10$ fs, they remain qualitatively unchanged for values of Δt up to 50 fs.

IV. POTENTIAL IMPLICATIONS

A. Interface formation

Our simulation results allow us to speculate about the likely reactions that govern the immediate interfacial chemistry of InP/GaP(001) in a photoelectrochem-

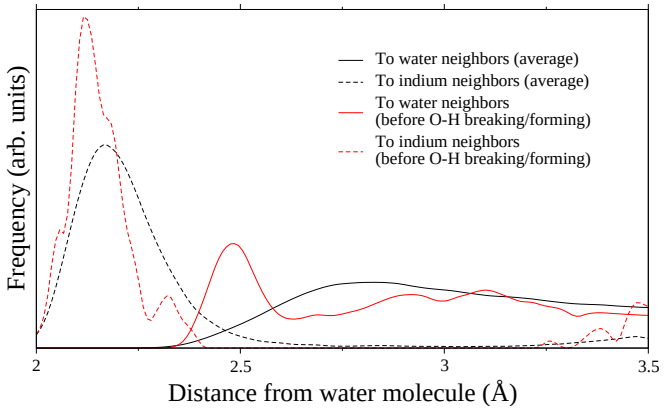

FIG. 8. Distribution of distances from water in the $L1$ region of OH-adsorbed InP(001) to neighboring water (solid lines) and surface indium atoms (dashed lines). Water locations are determined based on the location of the oxygen atom. Red lines are results for interfacial water molecules that break or form O–H bonds (forming OH^- or H_3O^+), sampled 10 fs prior to the bond breaking/forming event. Black lines are results averaged over all remaining frames.

ical cell. Prior to illumination, surface oxygen bridges are created through exposure to air or water. Upon immersion, these act as proton acceptors to promote dissociative adsorption of water molecules, which deposits additional oxygen and hydroxyl on the surface. To understand the significance of this, consider that under efficient cathodic operation, protons will be rapidly consumed via the evolution of H_2 gas. Depending on the active mechanism, the source of these protons could either be the surface itself, or else the solution (which will subsequently be rendered locally basic with respect to the bulk). Either way, the likely effect will be to encourage surface deprotonation. Because the simulations show deprotonation of surface hydroxyl groups to be kinetically feasible at room temperature, we assume that device operation will enhance the continuous regeneration of oxygen sites that can be used for further water dissociation. Accordingly, we propose that even small initial concentrations of surface oxygen will tend to nucleate dense surface hydroxylation via the mechanisms shown in Fig. 3.

Once the surface hydroxyl concentration is sufficiently high, a well-defined hydrogen-bond network is formed, and the interface enters a dynamic equilibrium with the solvent environment. However, the nature of this equilibrium differs significantly between GaP and InP. This is evident in the average surface compositions. For instance, GaP has a higher average concentration of surface oxygen bridges, whereas InP has a higher concentration of surface hydroxyl bridges (Table II). It is also evident in the dynamical fluctuations among different compositions and topologies, which tend to be much greater for InP. Both surfaces exhibit rapid surface hydrogen transfer between nearby In/Ga sites, aided by a weakening of O–H chemical bonds and a strengthening of O···H hydrogen bonds at the interface (Fig. 2). However, for GaP(001), the dynamics of surface hydrogen is largely limited to frequent local hopping events, due to the kinetic barriers associated with reorganization of the stiff interfacial hydrogen-bond network. On the other hand, InP(001) exhibits facile, solvent-driven network reorganization and rearrangement (Figs. 5 and 7). The InP(001)-water interface is therefore characterized by fluid, collective surface hydrogen transport, as well as continual exchange of $H/OH/H_2O$ with the solvent.

B. Kinetics of hydrogen evolution

We use our results to speculate about the probable kinetics of the overall hydrogen evolution reaction, including which steps may be rate limiting. This is best discussed in the more specific context of the Volmer-Heyrovsky-Tafel process, which is generally thought to underlie electrochemical hydrogen evolution.[53] In this model, the Volmer process first transfers an electron to an adsorbed proton. The reaction then proceeds either via the Heyrovsky process or the Tafel process. In the Heyrovsky process, a proton is donated from the solvent to an adsorbed hydrogen atom, which is coupled to an electron transfer reaction to form H_2. In the Tafel process, two adsorbed Volmer hydrogens combine via surface diffusion to form H_2.

The Volmer step is likely coupled to the dissociative adsorption of water, which according to our results is kinetically favorable at a bridge oxygen site on the semiconductor surface. Because experiments have established that surface oxygen is ubiquitous on as-grown GaP/InP(001) surfaces,[9,12–14,18] the rate of water dissociation is unlikely to limit the kinetics of the overall H_2 evolution reaction.

This insight has implications for understanding the role of metal surface catalysts, which are commonly deposited on III-V photocathodes to enhance reaction kinetics.[5,15,54,55] It is known that the catalyst acts as a current collector for electron transfer.[15,56,57] This is consistent with observations of Pt-decorated InP, where platinum improves surface stability by drawing current away from carrier-trapping sites.[15,58] However, its role in the other reaction steps of hydrogen evolution is less well understood. For instance, it is unclear whether water dissociation necessarily occurs at the catalyst surface, at the catalyst-semiconductor interface, or at active sites on the semiconductor surface. Our simulations suggest that because the InP/GaP(001) surface is able to dissociate water unaided, a metal surface catalyst is not required for this stage of the reaction. Rather, its role is to facilitate subsequent H_2 association and release. This agrees with reports on platinum, where a low barrier for surface hydrogen diffusion and H_2 association via the Tafel process has been demonstrated.[53]

Because InP(001) and GaP(001) demonstrate qualitatively different hydrogen transport behavior, this could translate to differences in the relevant hydrogen evolution mechanisms. We turn first to the scenario in which

hydrogen evolution proceeds via the Heyrovsky process. In this case, the hydrogen evolution rate will be limited by the proton-coupled electron transfer from the solvent to the hydrogen adsorbate. Here, our simulation results point to no obvious advantage of InP(001) over GaP(001), or vice versa. In general, this is the dominant mechanism for semiconductors when no catalyst is present and unaided electron transfer is relatively inefficient.[59,60]

However, if hydrogen evolution instead takes place via the Tafel process, then adsorbed hydrogens combine via surface diffusion to form H_2. This is very likely the case when an efficient surface catalyst is applied.[53,61] In this scenario, the role of the catalyst is to enable electron transfer, H–H bond formation, and H_2 release. Its performance is usually aided by a low hydrogen diffusion barrier on the catalyst surface. Here, we can imagine a potential benefit to having facile, long-range surface hydrogen transport of the sort exhibited by InP(001). It would allow the dissociation site at the semiconductor surface to be physically separated from the catalyst reaction site, where later stages of H_2 evolution occur. In other words, hydrogen from dissociated water could be shuttled to the catalyst-semiconductor interface. Otherwise, dissociation must occur directly at the catalyst-semiconductor interface, or else on the catalyst itself. This may help to explain why GaP does not show the same performance enhancement as InP upon addition of a platinum surface catalyst.[14,54]

Based on the above analysis of the Tafel process, we propose that the likely rate-determining mechanism in the presence of an efficient electron-transfer catalyst is the rate of surface hydrogen transport. Accordingly, fast, long-range surface transport of the sort exhibited by InP(001) may significantly improve electrode performance. Our proposal is consistent with various established experimental results on InP. One of these is the improved performance of InP photocathodes in acidic electrolytes, where surfaces are more likely to be protonated.[54,57,62] Similarly, it explains photovoltage improvements upon exposure of air-oxidized InP photocathodes to hydrogen-rich environments, as well as the reversal of such trends upon re-exposure to oxygen or application of positive potentials that strip away surface protons.[54,63,64] In addition, our proposal is consistent with the fact that increased areal catalyst density does not necessarily improve hydrogen evolution performance on InP.[15,54]

Our proposed model also clarifies seeming incongruities in a series of experiments relating the application of metal to a *p*-InP(001) surface. In one set of experiments in the presence of known high-performing catalysts, the onset potential for hydrogen evolution was found to depend only weakly on the catalyst type.[54,64] However, when metals with known poor catalytic activity were included in the analysis, the metal species essentially entirely determined the reaction kinetics and onset potential, and performance could actually be poorer than for the undecorated InP surface.[56,65] This points to the possibility of different governing mechanisms in the two regimes. Within our explanation, the presence of an efficient metal catalyst on InP(001) means the reaction would probably proceed via the Tafel process. The kinetics would therefore be limited by the surface hydrogen diffusion rate, rather than by the electron-transfer reaction. This would explain performance similarities between catalyst species. On the other hand, the reaction rate in the absence of an efficient catalyst should be determined by the Heyrovsky proton-coupled electron transfer reaction. In this case, any applied surface metal would collect available current, and the reaction site would be the three-way interface between the semiconductor, the metal, and the solution. The rate would therefore be determined largely by the electron transfer reaction at this junction, which depends strongly on the metal work function.

C. Corrosion

Previous reports in the literature have highlighted the favorable role of dilute surface oxygen adsorption in enhancing stability and kinetics of InP-based cells in an aqueous electrolyte.[7,15,17,62,66,67] The stabilizing behavior has been attributed to the passivation of surface states that can act as recombination sites. In these early reports, surface oxygen was sometimes proposed as the passivating agent. However, we find that the equilibrium concentration of water-exposed oxygen bridges at the InP surface is relatively low, and that passivation of surface sites is more likely to be driven by surface hydroxyl groups interacting strongly with interfacial water. Moreover, we previously showed that oxygen in a *M*–O–*M* bridge configuration has characteristics of a hole trap or surface recombination site upon application of local tensile strain.[19] This suggests that surface oxygen would be largely ineffective as a passivating agent.

If we assume that surface hydroxylation is the key passivating mechanism, we can speculate as to why GaP does not exhibit the same self-passivation behavior as InP, and why locally Ga-rich regions of the $GaInP_2$ alloy are less stable than locally In-rich regions.[9,14,15] The choice between the chemical pathways of corrosion/dissolution and passivation will depend on the thermodynamics and kinetics of the relevant processes during device operation. As such, we can extract clues from key differences between GaP and InP that we directly observe in the dynamics simulations.

First, the possibility of rapid, long-range surface hydrogen transport in InP(001) makes it especially easy to passivate dangling-bond surface states with hydrogen. This is because the hydrogen does not need to be provided directly at the dangling-bond site, but can instead be quickly shuttled from any available reaction site. We propose that this offers a self-passivating mechanism by which the surface can heal itself, as shown in Fig. 9a. Moreover, if an uneven distribution of charge builds up within the electrode—for instance, if one region becomes

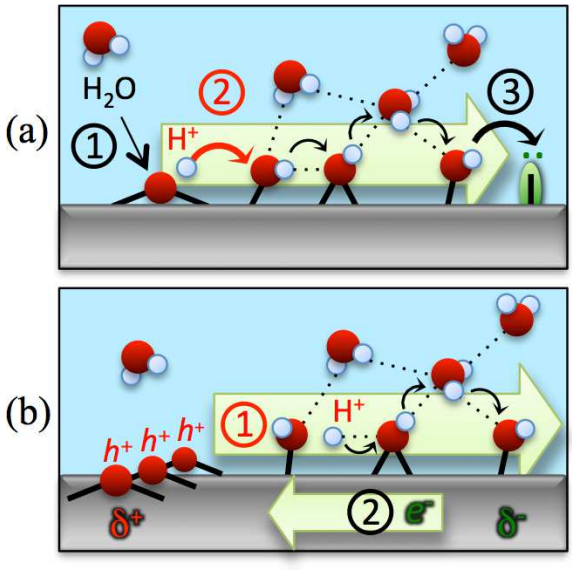

FIG. 9. (a) Schematic of the proposed self-healing mechanism on hydroxylated InP(001). Dissociative adsorption of water (#1) occurs at a reaction site away from the dangling bond (shown here in green). Rapid proton transport (#2) proceeds along the interfacial hydrogen-bond network to passivate the dangling-bond site (#3). (b) Schematic of two possible competing mechanisms for mitigating buildup of photogenerated potential differences within an InP(001) photocathode. In this example, illumination causes holes to accumulate at a region with high concentrations of strained M–O–M bridges, generating a locally positive bias. Charge compensation can happen by either by shuttling of surface protons towards regions of local negative bias (#1) or else by drawing electrons from ionized semiconductor atoms, thereby promoting corrosion (#2).

rich in dangling-bond states—then surface proton shuttling can also serve to quickly regulate and offset the resulting potential difference. This process can proceed much faster than proton donation from bulk water. This could be extremely important for the surface stability of InP(001), since it competes directly with galvanic corrosion. In galvanic corrosion, the potential difference is instead offset by drawing electrons from In or Ga atoms, which are ionized and solvated. Figure 9b illustrates these competing processes.

Turning next to purely thermodynamic considerations, we note that GaP(001) is energetically much more likely to have exposed surface M–O–M oxygen bridges than InP(001) (Table II). We previously discussed the possibility of strained oxygen bridges as nucleation sites for photocorrosion, although this has yet to be verified experimentally.[19]. In our proposed scenario, the p states of bridge oxygens become atomic like under local tensile strain, which leads to hole traps and carrier recombination sites under illumination. Uneven distribution of bridge oxygens will then generate a local anodic potential due to hole buildup, as in Fig. 9b. If surface oxygen bridges indeed play a role in photocorrosion, then higher native concentrations on GaP(001) would correspond directly to higher corrosivity. In the presence of a thin native surface oxide, environments that facilitate protonation of oxygen bridges should therefore exhibit improved passivation. This may contribute to the reported improved corrosion resistance in acidic electrolytes.[54,57,62]

Because corrosion mitigation remains a goal for the development of reliable III-V semiconductor photocathodes, we can use our insights to propose specific criteria for maintaining surface integrity. First, the formation of a fluid hydrogen-bond network with the capability for long-range hydrogen transport should be inherently beneficial. This provides a mechanism for self-healing of surface imperfections and potential differences. In systems such as hydroxylated InP(001), where long-range transport is present natively, the network should be retained when considering possible interface modifications. In systems such as GaP(001), where the network is too rigid, the surface should be tuned so as to weaken the interfacial hydrogen-bond strength. In doing so, one always needs to consider the tradeoff between the strength of the interfacial hydrogen-bond network and that of the interfacial O–H chemical bonds. Since favorable kinetics for local proton transfer and network reorganization are both necessary for long-range transport, there should be an ideal window of intermediate interfacial hydrogen and chemical bond strengths that should be targeted by electrolyte or electrode surface engineering.

Next, if strained oxygen bridges are nucleation sites for surface decomposition under illumination, then we could use chemically or mechanically induced local surface compression for surface stabilization. Because the strain effect is a highly local phenomenon, this would only need to impact the immediate metal-oxygen bond. Lattice strain may be an underlying contributor to the poor corrosion resistance of the surface Ga-rich regions of $GaInP_2$ compared to bulk GaP.[11] The larger lattice constant of $GaInP_2$ with respect to GaP would have the effect of inducing local tensile strain in Ga-rich areas of the surface, including any surface Ga–O bonds. One strategy would be be appropriately engineer the lattice constant by choice of the growth substrate. Another would be to accept the presence of strained oxygen bridges but ensure the grown oxide is sufficiently uniform and defect free so as to prevent buildup of the potential differences that lead to corrosion.

V. CONCLUSIONS

In conclusion, we have used *ab initio* molecular dynamics simulations of InP(001) and GaP(001) to investigate how the surface structure and chemistry changes upon contact with water. In order to simulate a more realistic electrochemical environment, we explicitly account for chemisorbed oxygen and hydroxyl at the surface. We find that the surface adsorbates fundamentally alter the interfacial properties. Adsorbed surface oxygen provides a

low-barrier pathway for water dissociation, whereas pristine InP/GaP(001) surfaces are kinetically inhibited towards dissociative water adsorption. Under device operation, dissociative adsorption at surface oxygen sites leads to a self-sustaining surface hydroxylation process that is active even for relatively small surface oxygen concentrations.

The hydroxylated surface is stabilized by hydrogen bonding with interfacial water. Despite similar electronic structures, InP and GaP exhibit fundamentally different interfacial dynamics. In particular, for InP(001), intermediate hydrogen-bond strength encourages local proton transfer while simultaneously permitting facile network reorganization capability. This allows for rapid long-range surface shuttling of hydrogen, which is kinetically unfavorable for GaP(001) due to the stiffness of its hydrogen-bond network.

We propose that long-range surface hydrogen transport allows the surface to efficiently passivate dangling bonds, which may contribute to the native corrosion resistance of InP. Moreover, fast surface hydrogen transport may enhance H_2 evolution by allowing water dissociation and H_2 formation to be physically separated (e.g., on the InP surface and Pt catalyst, respectively). Our interpretation is consistent with experimental observations on GaP and InP.

In light of our models, we suggest some broad strategies for mitigation of surface corrosion. These include the formation of a surface hydrogen-bond network with intermediate binding strength; the engineering of chemically or mechanically induced local compressive lattice strain; and the intentional growth of a carefully controlled surface oxide with minimal defects. We hope that these suggestions will aid future efforts towards improved durability and performance of III-V-based photoelectrodes.

The authors acknowledge helpful discussions with J. Turner, T. Deutsch, and H. Wang (NREL). Funding was provided by the U.S. Department of Energy Fuel Cell Technologies Program. Computing support came from the Lawrence Livermore National Laboratory (LLNL) Institutional Computing Grand Challenge program. This work was performed under the auspices of the U.S. Department of Energy by LLNL under Contract DE-AC52-07NA27344.

[1] U.S. Department of Energy, DOE BESAC Report (2008).
[2] A. Fujishima and K. Honda, Nature **238**, 37 (1972).
[3] N. S. Lewis and D. G. Nocera, PNAS **103**, 15729 (2006).
[4] J. Turner *et al.*, Int. J. Energy Res. **32**, 379 (2008).
[5] O. Khaselev and J. A. Turner, Science **280**, 425 (1998).
[6] S. Menezes, B. Miller, and K. J. Bachmann, J. Vac. Sci. Technol. B **1**, 48 (1983).
[7] H. Lewerenz and K. Schulte, Electrochim. Acta **47**, 2639 (2002).
[8] J. Vigneron, M. Herlem, E. M. Khoumri, and A. Etcheberry, Appl. Surf. Sci. **201**, 51 (2002).
[9] H. Wang and J. A. Turner, ECS Trans. **2**, 125 (2007).
[10] T. G. Deutsch, C. A. Koval, and J. A. Turner, J. Phys. Chem. B **110**, 25297 (2006).
[11] T. G. Deutsch, J. L. Head, and J. A. Turner, J. Electrochem. Soc. **155**, B903 (2008).
[12] O. Pluchery, Y. J. Chabal, and R. L. Opila, J. Appl. Phys. **94**, 2707 (2003).
[13] H. Morota and S. Adachi, J. Appl. Phys. **100**, 054904 (2006).
[14] B. Kaiser, D. Fertig, J. Ziegler, J. Klett, S. Hoch, and W. Jaegermann, Chem. Phys. Chem. **13**, 3053 (2012).
[15] A. Heller, Science **223**, 1141 (1984).
[16] W. E. Spicer, I. Lindau, P. Skeath, C. Y. Su, and P. Chye, Phys. Rev. Lett. **44**, 420 (1980).
[17] H. J. Lewerenz, D. E. Aspnes, B. Miller, D. L. Malm, and A. Heller, J. Am. Chem. Soc. **104**, 3325 (1982).
[18] G. Chen, S. B. Visbeck, D. C. Law, and R. F. Hicks, J. Appl. Phys. **91**, 9362 (2002).
[19] B. C. Wood, T. Ogitsu, and E. Schwegler, J. Chem. Phys. **136**, 064705 (2012).
[20] B. C. Wood, T. Ogitsu, and E. Schwegler, J. Photon. Energy **1**, 016002 (2011).
[21] R. Car and M. Parrinello, Phys. Rev. Lett. **55**, 2471 (1985).
[22] Giannozzi, P. *et al.*, J. Phys. Condens. Matt. **21**, 395502 (2009).
[23] G. J. Martyna, M. L. Klein, and M. E. Tuckerman, J. Chem. Phys. **97**, 2635 (1992).
[24] J. C. Grossman, E. Schwegler, E. W. Draeger, F. Gygi, and G. Galli, J. Chem. Phys. **120**, 300 (2004).
[25] D. Vanderbilt, Phys. Rev. B **41**, 7892 (1990).
[26] J. P. Perdew, K. Burke, and M. Ernzerhof, Phys. Rev. Lett. **77**, 3865 (1996).
[27] Y. Zhao and D. G. Truhlar, J. Chem. Theory Comput. **1**, 415 (2005).
[28] W. L. Jorgensen, J. Chandrasekhar, J. D. Madura, R. W. Impey, and M. L. Klein, J. Chem. Phys. **79**, 926 (1983).
[29] W. G. Schmidt, Appl. Phys. A **75**, 89 (2002).
[30] N. Marzari and D. Vanderbilt, Phys. Rev. B **56**, 12847 (1997).
[31] N. Marzari, A. A. Mostofi, J. R. Yates, I. Souza, and D. Vanderbilt, Rev. Mod. Phys. (2012), in press.
[32] D. Marx, ChemPhysChem **7**, 1848 (2006).
[33] K. C. Hass, W. F. Schneider, A. Curioni, and W. Andreoni, Science **282**, 265 (1998).
[34] S.-C. Li, Z. Zhang, D. Sheppard, B. D. Kay, J. M. White, Y. Du, I. Lyubinetsky, G. Henkelman, and Z. Dohnálek, J. Am. Chem. Soc. **130**, 9080 (2008).
[35] H. S. Kato, K. Akagi, S. Tsuneyuki, and M. Kawai, J. Phys. Chem. C **112**, 12879 (2008).
[36] G. Cicero, G. Galli, and A. Catellani, J. Phys. Chem. B **108**, 16518 (2004).
[37] J. Wang, L. S. Pedroza, A. Poissier, and M. V. Fernandez-Serra, J. Phys. Chem. C **116**, 14382 (2012).
[38] C. Sun, L.-M. Liu, A. Selloni, G. Q. M. Lu, and S. C. Smith, J. Mater. Chem. **20**, 10319 (2010).
[39] S. Meng, E. G. Wang, and S. Gao, Phys. Rev. B **69**, 195404 (2004).
[40] J. Carrasco, A. Hodgson, and A. Michaelides, Nature Mater. **11**, 667 (2012).
[41] A. B. Muñoz García and E. A. Carter, J. Am. Chem. Soc. **134**, 13600 (2012).
[42] N. Gayathri, S. Izvekov, and G. A. Voth, J. Chem. Phys. **117**, 872 (2002).
[43] O. Henrion, A. Klein, and W. Jaegermann, Surf. Sci. **457**, L337 (2000).
[44] G. Henkelman, B. P. Uberuaga, and H. Jonsson, J. Chem. Phys. **113**, 9901 (2000).
[45] NEB calculations were based on seven images to describe the minimum-energy reaction path, using climbing images.
[46] S. Jeon, H. Kim, W. A. Goddard III, and H. A. Atwater, J. Phys. Chem. C **116**, 17604 (2012).
[47] A history-dependent hysteresis was applied for evaluating the existence of an O–H chemical bond: an existent bond was considered to break for interatomic distance d(O–H)$\geq$ 1.40 Å, whereas the criterion for new O–H bond formation was d(O–H)$\leq$ 1.15 Å. This prevented overcounting of bond breaking events due to thermal bond stretching.
[48] G. Cicero, J. C. Grossman, A. Catellani, and G. Galli, J. Am.

Chem. Soc. **127**, 6830 (2005).
[49]M. Sumita, C. Hu, and Y. Tateyama, J. Phys. Chem. C **114**, 18529 (2010).
[50]B. C. Wood and N. Marzari, Phys. Rev. B **76**, 134301 (2007).
[51]A. Vittadini, A. Selloni, F. P. Rotzinger, and M. Grätzel, Phys. Rev. Lett. **81**, 2954 (1998).
[52]X. Shen, Y. A. Small, J. Wang, P. B. Allen, M. V. Fernandez-Serra, M. S. Hybertsen, and J. T. Muckerman, J. Phys. Chem. C **114**, 13695 (2010).
[53]J. O. Bockris and S. U. M. Khan, *Surface Electrochemistry: A Molecular Level Approach* (Plenum Press, New York, 1993).
[54]A. Heller, E. Aharon-Shalom, W. A. Bonner, and B. Miller, J. Am. Chem. Soc. **104**, 6942 (1982).
[55]M. A. Butler and D. S. Ginley, Appl. Phys. Lett. **42**, 582 (1983).
[56]M. Szklarczyk and J. O. Bockris, J. Phys. Chem. **88**, 5241 (1984).
[57]A. Bansal and J. A. Turner, J. Phys. Chem. B **104**, 6591 (2000).
[58]P. Bogdanoff, P. Friebe, and N. Alonso-Vante, J. Electrochem. Soc. **145**, 576 (1998).
[59]J.-N. Chazalviel, A. Beladi, M. Safi, F. Maroun, B. Ern, and F. Ozanam, Electrochim. Acta **45**, 3205 (2000).
[60]Y. Li, H. Wang, L. Xie, Y. Liang, G. Hong, and H. Dai, J. Am. Chem. Soc. **133**, 7296 (2011).
[61]B. Conway and B. Tilak, Electrochim. Acta **47**, 3571 (2002).
[62]O. Khaselev and J. A. Turner, J. Electrochem. Soc. **145**, 3335 (1998).
[63]D. E. Aspnes and A. Heller, J. Phys. Chem. **87**, 4919 (1983).
[64]A. Heller, J. Phys. Chem. **89**, 2962 (1985).
[65]J. O. Bockris and R. C. Kainthla, J. Phys. Chem. **89**, 2963 (1985).
[66]S. Menezes, H. J. Lewerenz, F. A. Thiel, and K. J. Bachmann, Appl. Phys. Lett. **38**, 710 (1981).
[67]A. Heller, B. Miller, H. J. Lewerenz, and K. J. Bachmann, J. Am. Chem. Soc. **102**, 6555 (1980).